## Nanomechanical properties of individual chondrocytes and their developing growth factor-stimulated pericellular matrix

### Appendix (Supplementary Material)

*Appendix A. Experimental quantification of the rate-dependence of indentation hysteresis of individual chondrocytes*

Freshly isolated cells were probed with the nanosized and micron-sized tips at indentation rates of 200nm/s, 500nm/s, 1μm/s, 3μm/s, and 5μm/s. The area enclosed by the hysteresis loop (e.g., Fig. 6) is related to the strain energy dissipated during cyclic loading of the cell, which is most likely associated with viscoelastic and/or poroelastic cell behavior (Leipzig and Athanasiou 2005). The hysteresis loop area was calculated by fitting the loading and unloading curves to polynomials, integrating, and subtracting the area under the unloading from that of the loading curve. Hysteresis was seen at all rates and normalized to the area obtained at 1μm/s (Fig. A1). In this study, an increase in hysteresis was not seen between 200nm/s to 1μm/s indentation rates, indicating a pseudo-steady state within this loading regime, giving an estimated relaxation time constant of ~1s (based on a rate of 1μm/s). A previous study involving cytoindentation of single adult bovine chondrocytes reported a time relaxation constant of 1.32s (Koay et al., 2003). Similar hysteresis behavior was reported previously for skeletal muscle cells for

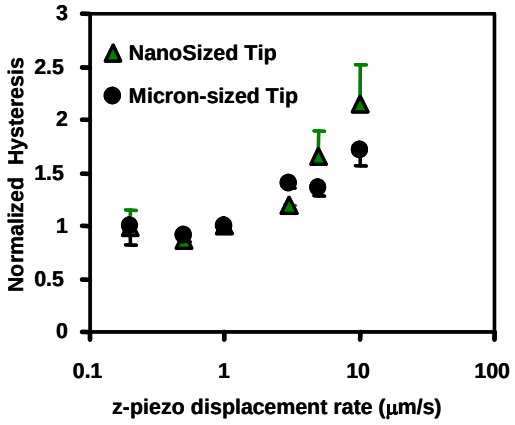


Fig A1. Average hysteresis area (mean ± SE) normalized to the hysteresis area measured for cells using a displacement rate of 1μm/s with the nanosized tip (n = 6 cells, each with five sequential loading and unloading curves) and micron-sized tip (n = 4, each with five loading and unloading curves). Minimal change in hysteresis was observed between displacement rates of 200nm/s to 1μm/s.

which hysteresis did not decrease below 500nm/s (Collinsworth et al., 2002). We therefore used

1μm/s z-piezo displacement for data collection. Hysteresis was thereby minimized in order to reduce the contribution of cell visco- and poroelastic dissipation and thereby calculate the apparent elastic properties of the cell (A-Hassan et al., 1998).

*Appendix B. Theoretical modeling of indentation of individual chondrocytes for the estimation of apparent elastic moduli*

*B.1. Hertz model (isotropic elastic half-space)*

Using the small strain region (ε<0.05) corresponding to an indentation depth up to 300 nm for the data of Fig.7, the Hertz model was used to calculate an apparent modulus for the nanosized and micron-sized tip. The modified Hertz model of a rigid conical probe tip in contact with an elastic material was used for the nanosized tip indentation (Radmacher 1997):

$$F = \frac{\pi}{2}\frac{E}{(1-\nu^2)} D^2 \tan\alpha \qquad (A1)$$

where $F$ = force (nN), D = indentation depth (μm), E = Young's modulus (cell, kPa), $\upsilon$ = Poisson's ratio (taken as 0.4 (Freeman et al., 1994), and probe tip angle $\alpha$ = 35°. The $Si_3N_4$ tip (modulus~400GPa (Petersen 1982)) can be assumed rigid compared to the cell (modulus ~1kPa). This model gave an average modulus E = 0.85 kPa (Fig. A2a). Matching the Hertz model to the upper and lower limits of the standard error gave a modulus range between 0.7kPa to 1.0kPa (Table A1).

For the micron-sized tip, the Hertz model of two contacting spheres was used assuming a rigid colloidal tip and an elastic cell (Johnson and Greenwood 1997):

$$F = \frac{4}{3}\frac{E}{(1-\nu^2)}\sqrt{\frac{1}{\frac{1}{R_1}+\frac{1}{R_2}}}\, D^{3/2} \qquad (A2)$$

where $R_1$ = radius of micron-sized tip (μm) and $R_2$ = radius of cell = 7.65 μm. The Hertz model compared well to the experimental data with a modulus of 1kPa

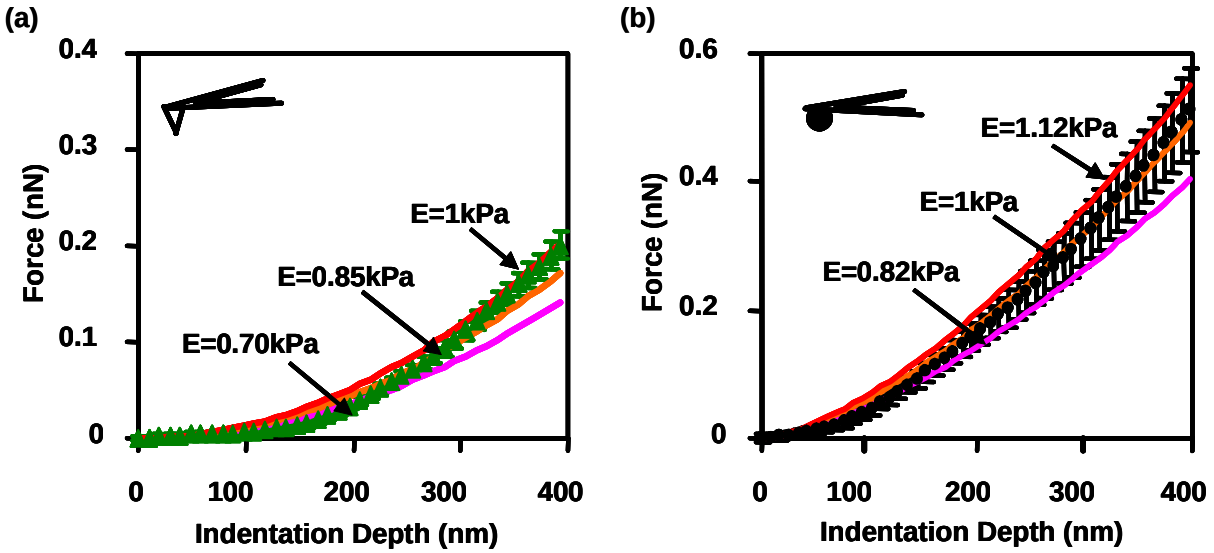


Fig. A2. Comparison of experimental data up to 400 nm indentation distance (from Fig. 7, freshly isolated calf chondrocytes) to the predictions of the Hertz model using , $R_{cell}$ =7.6 μm, Poisson's ratio=0.4, for (a) the nanosized and (b) the micron-sized tip, respectively. Indentation curves on loading (mean ± SE) taken with both the nanosized (average of 25 cells with 5 loading cycles/cell, $R_{tip}$ ~ 40nm) and micron-sized (average of 17 cells with 5 loading cycles/cell, $R_{tip}$ ~ 2.5μm) probe tips. Based on the data, the modulus used in the Hertz model was chosen to bracket the data of the force-indentation curves.

(Fig. A2b). The upper and lower limits matched the standard error with moduli of 1.12kPa and 0.82kPa, respectively.

The apparent moduli of 0.70 - 1.00 kPa and 0.82 - 1.12 kPa for the nanosized and micron-sized tips, respectively, were significantly different ($p<0.05$, unpaired t-test). These values are in the range between 0.65 - 2.47 kPa reported previously using micropipette aspiration (Jones et al., 1999) and unconfined compression (Leipzig and Athanasiou 2005). Interestingly, the apparent elastic cell moduli estimated from our nanosized tip data were significantly lower than those estimated from the micron-sized probe tip data. Previous studies have also emphasized differences in matrix (Stolz et al., 2004) and cellular properties (Lehenkari et al., 2000b) measured at nano- versus and micron- length scales. Of course, all such elastic models are based on the simplifying assumption that the cell can be represented as a homogeneous elastic solid. It should be noted that while we assume a simple elastic model, the hysteresis seen with both probe tips (Fig. 6) indicated that more complex viscoelastic and/or poroelastic behavior was present. Ongoing studies are focused on estimation of poro-viscoelastic cell parameters from these data.

*B.2. Stress-strain*

A stress-strain (σ-ε) curve was calculated from the force-indentation depth data of Fig. 7 using the 0 - 200 nm depth range for the micron-sized tip. The stress was calculated by dividing force by a contact area that increased with indentation depth.

$$\sigma = \frac{F}{A} \quad \text{and} \quad \varepsilon = \frac{D}{2R_2} \qquad (A3)$$

where $A = 2\pi R_1 D$. A modulus of 1.96 kPa was calculated from the slope of the σ-ε curve (Fig. A3), which was linear in this range. The Hertz model and stress-strain estimation for the micron-sized probe tip yielded similar apparent moduli for freshly isolated chondrocytes. Due to the complex contact interaction between the sharp nanosized tip and the cell, an accurate stress-strain curve could not be estimated.

*B.3. Finite element analysis: Effect of mesh density and boundary conditions*

Finite element analysis was used only for the micron-sized tip as the nanosized tip simulations had difficulty converging at depths larger than 150nm due to its small radius of curvature relative to the indentation depth. The fixed parameters were probe

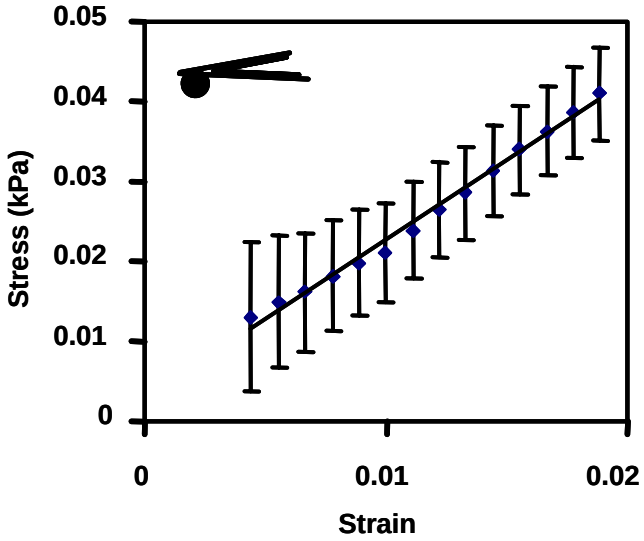


Fig. A3. Stress-strain curves for nanoindentation data shown in Fig. 7 for loading (mean ± SE) for freshly isolated calf chondrocytes (day0) taken with micron-sized probe tips (average of n=17 cells with 5 loading cycles/cell, $R_{tip}$~2.5 μm) resulting in an average E=1.96kPa with a range of 1.76-2.19 kPa.

tip end-radius of 2.5μm, cell diameter of 7.6 μm, and Poisson's ratio of 0.4 (Freeman et al., 1994;Jones et al., 1999). The fitting parameter was the cell modulus. Contact between the indenter and cell was frictionless. A 20-node quadratic brick mesh (C3D20 in ABAQUS element library) was seeded with a higher density in the vicinity of the contact region of the probe tip where larger stresses and strains occurred. To verify that the mesh was dense enough to obtain accurate results, two different densities of meshes were implemented and showed agreement of the resultant F-D curves. Boundary conditions may also influence the FEA results. The exact interaction between the cell and well wall are unknown, so the two extremes of no-slip and frictionless boundary conditions were implemented. Interestingly, a no-slip boundary condition between the elastic cell and rigid wall resulted in a lower modulus (by ~25%) compared to the frictionless boundary condition. This implies that if the wall is frictionless, then the tip has to indent more of the cell to obtain an equally large resultant force to that of the no-slip wall, which may be due to the cell "slipping" into the well.

*B.4. Cell-PCM elastic two-layered finite element analysis*

The elastic cell, 7.6μm diameter, was modeled with a modulus of 2.75kPa. The elastic PCM was modeled as being 3.65μm thick with the modulus used as the fitting parameter. A PCM modulus of 4.15 kPa was needed to match the experimental data, consistent with the observation that IGF-1+OP-1 treatment produced much stiffer cells-PCM composites by day 28. At an indentation distance of 860 nm, the cell was more deformed (0.155 μm vs. 0.014 μm) when surrounded by the stiffer PCM. The softer PCM absorbed the indentation force and did not cause cell deformation as readily as the stiffer PCM. Interestingly, the deformation of the PCM by the tip was approximately the same for both the 0.1 kPa and 4.15 kPa PCM stiffness (0.63 μm vs. 0.59 μm, respectively).

*B.5. Viscoelastic and poroelastic models*

Quasi-static viscoelastic models to predict creep and stress relaxation behavior and to extract instantaneous and equilibrium moduli, viscosity, and a relaxation time constant have been developed in the area of nanoindentation of polymeric films such as polystyrene, semicrystalline polyvinyl alchohol (Cheng et al., 2005), and poly(methyl methacrylate) (PMMA), and poly (dimethylsiloxane) (PDMS) (Oyen and Cook 2003;VanLandingham et al., 2005). A similar approach has been used along with unconfined compression tests to estimate parameters for individual chondrocytes (Leipzig and Athanasiou 2005;Shieh and Athanasiou 2005). By applying small sinusoidal oscillations (2-50 nm amplitude at 0.1 - 300 Hz), dynamic viscoelastic models have been used to calculate storage and loss moduli of PMMA and PDMA films via nanoindentation (White et al., 2005). Dynamic testing has also been performed via AFM with a colloidal probe tip for single cells such as fibroblasts (Mahaffy et al., 2004), alveolar epithelial cells(Rico et al., 2005), and smooth muscle cells (Smith et al., 2005), and using a nanosized pyramidal tip for lung epithelial cells (Alcaraz et al., 2003). In these approaches, the form of the elastic Hertz model was extended to incorporate time-dependent behavior and thereby derive viscoelastic material parameters. Poroelastic models, which include the spatial and temporal dependence of fluid-solid frictional interactions and intracellular pressure

gradients to characterize time dependent cell deformation behavior, have also been used to predict the effective equilibrium elastic modulus and the hydraulic permeability of single chondrocytes, modeled as homogeneous, linear, isotropic biphasic media in unconfined compression (Leipzig and Athanasiou 2005). The recent experimental identification of non-equilibrium intracellular hydrostatic pressure gradients within the cytoplasm, or blebs, of filamin-depleted melanoma cells (Charras et al., 2005) have, indeed, suggested that such poroelastic behavior may be intrinsic to transient or dynamic cell deformation.

Motivated by the observed hysteresis in our nanoindentation experiments, we first used the simple three-element viscoelastic solid model of Eq. (A4) (Leipzig and Athanasiou 2005) to calculate effective viscoelastic parameters corresponding to the micron-sized tip data of Fig. 6b:

$$\frac{1}{E(t)} = \frac{1}{E_\infty} + \frac{E_\infty - E_0}{E_0 E_\infty} e^{-t/\tau} \qquad (A4)$$

Using a value for the relaxed modulus, $E_\infty$ = 1 kPa, corresponding to effective equilibrium modulus predicted from the Hertz model derived from the data of Fig. A2b, the hysteresis loop area at a loading rate of 1 μm/s data (i.e., Fig. 6b) was reasonably well matched using parameter values for the instantaneous modulus, $E_0$ = 2 kPa and the time constant $\tau$ = 0.1 s. Interestingly, these values of $E_\infty$ , $E_0$ , and $\tau$ are all within a factor of 2-3 of those reported by Leipzig and Athanasiou, 2003. We note, however, that these calculated values were found to vary with loading rate, as the measured hysteresis (Fig. A1) did not increase proportionally with loading rate. Therefore, our ongoing studies focus on extensions using dynamic viscoelastic models to calculate frequency-dependent storage and loss moduli ($G'(\omega)$, $G''(\omega)$) describing the relaxation spectrum as well as poroelastic models that incorporate both time and space dependence as well as nonlinear behavior.

| | | Nanosized Probe Tip Average | SE Interval | Micron-sized Probe Tip Average | SE Interval |
|---|---|---|---|---|---|
| **Day 0 (Freshly Isolated Cells)** | **Hertz Model** | 0.85 kPa | 0.7-1 kPa | 1.0 kPa | 0.8-1.12 kPa |
| | **Stress-Strain** | --- | --- | 1.96 kPa | --- |
| | **FEA** | --- | --- | 2.75 kPa | 2.3-3 kPa |
| **Day 21 PCM** | **FEA : FBS** | --- | --- | 0.1 kPa | 0.07-0.12 kPa |
| | **FEA : IGF-1 +OP-1** | --- | --- | 1.0 kPa | 0.8-1.3 kPa |
| **Day 28 PCM** | **FEA : FBS** | --- | | 0.17 kPa | 0.1-0.2 kPa |
| | **FEA : IGF-1 +OP-1** | --- | | 4.15 kPa | 3.75-4.70 kPa |

Table A1. Summary of apparent cell moduli obtained by comparison of experimental data of Figure 10b with three different models. For nanosized tip, a modulus could not be calculated with the stress-strain curve due to the complex contact interaction of the sharp tip radius and the cell. The FEA simulation with the nanosized tip also had trouble converging due to the probe's small radius of curvature relative to the indentation depth. For the day 21 and day 28 cells, the cell modulus was set to 2.75kPa while the PCM was varied until the FEA F-D matched the experimental data.